Bioderived Ionic Liquids with Alkaline Metal Ions for Transient Ionics

*Shunsuke Yamada**

Shunsuke Yamada[1]

[1]Department of Robotics, Division of Mechanical Engineering, Tohoku University, 6-6-01 Aoba, Aramakiaza, Aobaku, Sendaishi, Miyagi, 980-8579, Japan

*Corresponding author, e-mail: santa@tohoku.ac.jp

Keywords: Bioderived material, Ionic liquid, Ionic gel, Electrolyte, Transient electronics,

Abstract

An ionic liquid, choline lactate, composed of bioderived materials, offers an opportunity to develop electrochemical devices which degrade after use. Although ionic liquids show large potential windows, high ionic conductivity, and non-volatility, the ionic liquids do not show electrochemical characteristics – intercalation pseudo-capacitance, redox pseudo-capacitance, and electrochromism, for example. We, therefore, develop bioderived ionic liquids including biodegradable metal ions, Li, Na, and Ca, to yield ionic liquids electrochemical behaviors. Differential scanning calorimetry reveals that the ionic liquids remain in liquid states with a temperature range from 230.42 K to 373.15K. The ionic liquids with metal ions show lower ionic conductivities than that of the pristine ionic liquid whereas the influence of the ions on capacitances is negligibly small. A biodegradability test based on a protocol of Organization for Economic Co-operation and Development 301C modified MITI test (I) confirms that the pristine ionic liquid and those with the metal ions, and an ionic gel composed of the ionic liquid and poly(vinyl alcohol) exhibit ready biodegradability and biodegradability, respectively. The electrochromic device was developed using the ionic liquid with the Li ions. The device successfully changes the color with a voltage of −2.5 V by the intercalation of the Li ions into the WO_3 crystal. The results are of interest as the biodegradable ionic liquids with metal ions for electrochemical devices in research fields including environmentally benign devices, sustainable electronics, and bioresorbable/implantable devices, that conventional ionic liquids are unable to achieve.

1. Introduction

With the development of an emerging scheme of transient electronics, devices that decompose after a prescribed time have a great interest for applications including environmental sensing and implantable devices. Transient devices, transistors[1], sensors[2], and batteries[3] have been developed, using biodegradable organic and inorganic materials. Ionic liquids (ILs) solely composed of ions show non-volatility, high ionic conductivity, and electrochemical stability, and some ionic liquids, furthermore, possess biodegradability[4] and are favorable for energy storage devices for such electronics. Upon application of voltage, ions of the ionic liquids are attracted to electrodes and form an extremely thin layer, so-called, an electrical double layer[5]. The carbon electrodes show a large accessible surface area of ions, which leads to the large electrical double layer capacitance[6].

In addition to the electrical double layer capacitance, a capacitive behavior associated with a faradic or redox reaction is desired to enhance capacitance [7]. A Transition metal oxide, MoO_3, possesses a layered crystalline structure that has tiny gaps, van der Waals gaps[8] (vdW gap), and can accommodate tiny ions. Upon immersion of an electrode with the metal oxides into electrolytes containing sodium (Na) ions, the ions absorb and desorb onto the surface of the oxide; ions are, furthermore, intercalated and deintercalated into the vdW gap. Such absorption and intercalation show a capacitive behavior, known as intercalation pseudo-capacitance[8-9]. The MoO_3 electrode shows biocompatibility and biodegradability, and researchers reported biodegradable pseudo-capacitors using MoO_3 as the electroactive material[3, 8a, 10]. The aqueous electrolytes in the aforementioned works consist of salts and water which are present in human bodies, and therefore the electrolytes are promising materials for implantable and bioresorbable devices. Evaporation of water is, however, inevitable for such electrolytes, and previous works, therefore, doped metal ions, such as Li, Na, and potassium (K), into ILs for electrochemical devices[11]. Those ILs are toxic to provide adverse effects on the human body and environment, which prevents biodegradable and biocompatible applications of the ILs. To address this issue,

we have developed a bio-derived IL with the Na ions for an electrolyte for a pseudo-capacitor. The IL, 2-hydroxyethyl-trimethylammonium L-lactate ([Chol][Lac]) is composed of choline[12] and lactic acid[13] which are essential elements for human bodies. Choline which is present in foods, drugs, and bodies, is classified as a nutrient by the National Institutes of Health (NIH)[14]. Lactate also exist in the human body and is one of the final products to derive energy from glucose after the processes of fermentation and respiration[15]. In our previous work, sodium lactate ([Na][Lac]) was added to the IL as the Na source, and the Na ions intercalate into the vdW gap of MoO_3 to lead to three times larger capacitance of 1.5 mF/cm^2 than that without Na ions[16]. While we successfully confirmed the electrochemical behavior using the triple-ion system ([Chol][Na][Lac]), lactic acid has the salt family including Li, Na, and Ca, and a comprehensive study of electrochemical and biodegradable characteristics on the IL with the alkaline metal ions are essential for the transient ionics, including batteries, sensors, and electrochromic devices.

Herein, we report a bioderived IL with Li, Na, and Ca ions for transient ionics. As shown in **Fig. 1a**, salts which have the same anion specie as that of an IL dissolves into the IL. In this work, we dissolved the salts, lithium-L-lactate ([Li][Lac]), sodium-L-lactate ([Na][Lac]), and calcium lactate ([Ca][Lac]) into the pristine IL (PIL) with the weight ratio of 5wt%, 10wt%, and 15wt%. Unless otherwise noted, the ILs which include Li, Na, and Ca ions are referred to as ILLi, ILNa, and ILCa, respectively, where the superscript number denotes the weight ratio of the salt. The PIL, ILLi, ILNa, and ILCa show low glass temperatures of less than 233 K (–43˚C) and no peaks associated with endothermic or exothermic, which indicates that the ILs remain stable as liquids within a temperature range from –43˚C to 100˚C. With the increase of the weight ratios of the salts, whereas the ILs decrease ionic conductivities, capacitances and potential windows of the ILs show negligible change. Degradation of the PIL, $ILLi_5$, $ILLi_{10}$, $ILNa_5$, $ILNa_{10}$, $ILNa_{15}$, $ILCa_5$, $ILCa_{10}$, $ILCa_{15}$ and an ionic gel (IG) composed of 20wt% PVA and the 80wt% PIL were investigated based on OECD guidelines for testing of chemicals

(OECD 301C modified MITI test (I)). According to biological oxygen demand (BOD), the biodegradability of the ILs more than 69% after the tests. A dissolved organic carbon DOC measurement reveals that the ILs show biodegradability of more than 92.9% 28 days after the incubation, which indicates that the ILs are classified as ready biodegradability. PVA shows slow biodegradation that leads to the result that the IG is not classified as ready biodegradability; its biodegradability and water-dissolution are beneficial for solid-state ionic devices. The $ILLi_{10}$ was added into the PVA with weight ratio of 20wt% and 80wt%, respectively, to develop an electrochemically active electrolyte, and we have developed the electrochromic device (EC) using the IG, WO_3, and FTO, as the electrolyte, electrochemical active layer, and transparent electrode, respectively. The EC changes the transmittance by 30% with a voltage of −2.5 V, and the coloration efficiency η is 18 cm^2/C.

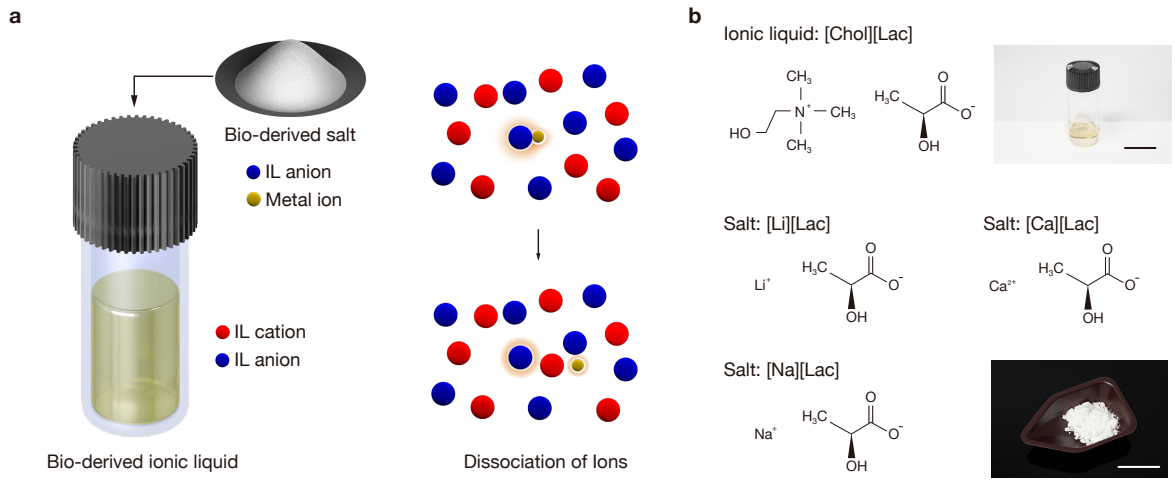

Figure 1. (a) Schematic of dissolution of the salt into the ionic liquid. (b) Photographs and chemical formulas of the pristine ionic liquid ([Chol][Lac], scale bar 20 mm) and salts ([Li][Lac], [Na][Lac], and [Ca][Lac], scale bar 20 mm).

2. Results and Discussion

2.1. Preparation of Ionic Liquids.

Firstly, vacuum annealing at 70˚C for 24 h removed residual moisture in the PIL and salts. A magnetic stirrer vigorously mixed the PIL and salts to dissolve, where the weight ratios of the salts were 5wt%, 10wt%, and 15wt% with regard to the IL. **Table 1** summarizes the ILs, weight ratios of salts, and mole fractions. The mole fraction M_f is defined as

$$M_f = \frac{[X][Lac]}{[Cho][Lac] + [X][Lac]}, \quad (1)$$

where [X][Lac] (X = Li, Na, or Ca) and [Cho][Lac] are moles of the salts and IL, respectively. It should be noted that the 15wt% [Li][Lac] did not dissolve into the IL, and hence the liquid, $ILLi_{15}$ was not subject to the following experiments.

Table 1. Weight ratio and mole fraction of the metal ions.

No.	Name	Metal ion	Weight percentage of salt (wt%)	Mole fraction of metal ion
1	PIL	-	0	0
2	$ILLi_5$	Li	5	0.096
3	$ILLi_{10}$	Li	10	0.18
4	$ILLi_{15}$	Li	15	0.26
5	$ILNa_5$	Na	5	0.083
6	$ILNa_{10}$	Na	10	0.16
7	$ILNa_{15}$	Na	15	0.23
8	$ILCa_5$	Ca	5	0.045
9	$ILCa_{10}$	Ca	10	0.090
10	$ILCa_{15}$	Ca	15	0.14

2.2. Thermal Characteristics

Figure 2a, **2b**, and **2c** show differential scanning calorimetry (DSC) curves of the ILLis, ILNas, and ILCas, respectively. The ILs were cooled down to 143 K (–130˚C) and heated up to 373 K (100˚C) at a scan rate of 10 K/min. The glass transition of PIL is 215.29 K (–57.86˚C), but peaks associated with neither endothermic nor exothermic processes are observed during the heating scan. The curves of ILLis, ILNas, and ILCas are similar to that of the PIL. The glass

transition temperatures are summarized in **Table 2**. Except for the IL with the Li salt, the temperatures rise more than 10 K with the IL with the 15wt% salt. The ILs remain in the liquid state with a temperature ranging from –43˚C to 100˚C, which indicates that devices using the ILs can operate under extreme environments[17].

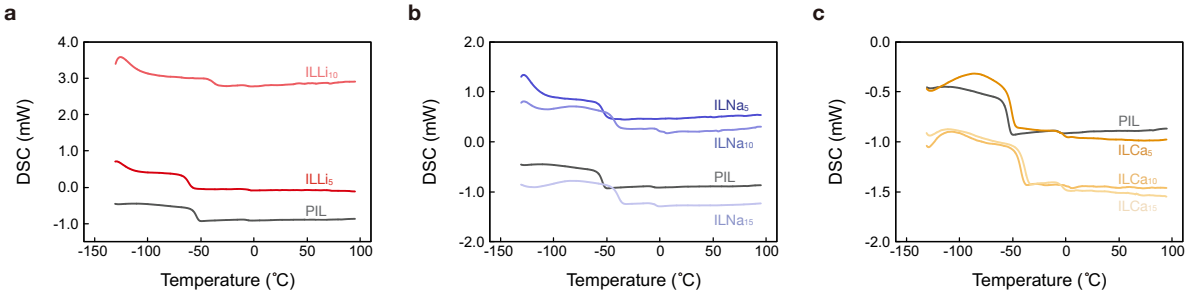

Figure 2. Differential scanning calorimetry profiles of the (a) [Li][Lac], (b) [Na][Lac], and (c) [Ca][Lac], with a temperature range from -140˚C to 100˚C at a scan rate of 10 K/min.

Table 2. Glass transition temperatures of the ionic liquids.

Ionic liquid	Glass transition temperature
PIL	215.29 K (–57.86˚C)
$ILLi_5$	207.77 K (–65.38˚C)
$ILLi_{10}$	230.42 K (–42.73˚C)
$ILLi_{15}$	-
$ILNa_5$	215.59 K (–57.56˚C)
$ILNa_{10}$	226.50 K (–46.65˚C)
$ILNa_{15}$	229.02 K (–44.13˚C)
$ILCa_5$	218.16 K (–54.99˚C)
$ILCa_{10}$	226.25 K (–46.90˚C)
$ILCa_{15}$	229.73 K (–43.42˚C)

2.3. Electrochemical measurement.

We performed electrochemical impedance spectroscopy (EIS) on the PIL, ILLis, ILNas, and ILCas, to investigate the influence of salt dissolution on ionic characteristics. **Figure 3a**, **3b**, and **3c** shows schematic illustration, photograph, and electrical connection of the experimental

bed, respectively. A pair of electrodes were assembled using a glass spacer with the thickness of 500 μm, followed by injection of the ILs through holes. **Figure 3d**, **3e**, and **3f** show absolute impedance |***Z***| and phase $\boldsymbol{\theta}$ of the ILLis, ILNas, and ILCas, respectively, with a frequency ranging from 10 mHz to 1 MHz. The |***Z***| in a high frequency regime increases with an increase in weight ratio of the salt. The $\boldsymbol{\theta}$ in high frequency and low frequency regimes decreases and increases, respectively. **Figure 3g**, **3h**, and **3i** summarize the ionic conductivities $\boldsymbol{\sigma}$s of ILLis, ILNas, and ILCas, respectively, defined as:

$$\sigma = \frac{t}{AR}, \qquad (2)$$

where $\boldsymbol{t}$, $\boldsymbol{A}$, and $\boldsymbol{R}$ are the gap between the electrodes, contact area at the interface of the IL and the electrodes, and resistance at 100 kHz, respectively[18]. The PIL exhibits the $\boldsymbol{\sigma}$ of 163 μS/cm; the $\boldsymbol{\sigma}$s of the $ILLi_{10}$, $ILNa_{15}$, and $ILCa_{15}$ decrease to be 29 μS/cm, 34 μS/cm, and 28 μS/cm, respectively, with an increase in the weight ratios. The dissolution of the Na ions into the PIL lowered the $\boldsymbol{\sigma}$ in our previous work, which results from an increase in the viscosity of the ILs by the enhancement of an interaction between the Na ion and [Lac] [19]. The Li and Ca ions enhance such interaction to reduce the ionic conductivities.

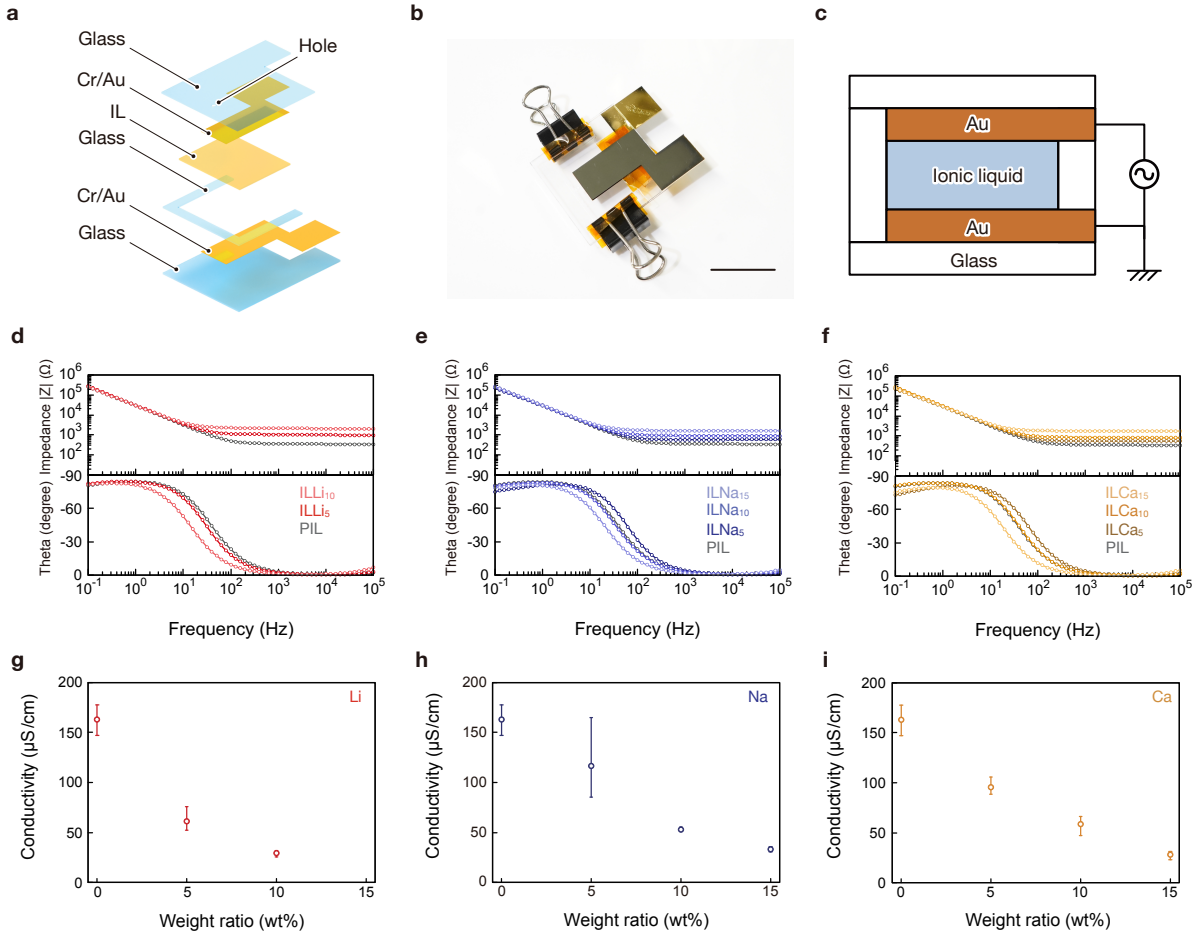

Figure 3. Electrochemical measurement on the ionic liquids (ILs). (a) Schematic and (b) photograph of the experimental setup (scale bar 20 mm). (c) Electrical connection diagram of the device. Bode diagrams of the (d) ILLis, (e) ILNas, and (f) ILCas with a frequency ranging from 10 mHz to 1 MHz. The ionic conductivities of the (g) ILLis, (h) ILNas, and (i) ILCas ions at 100 kHz.

Figure 4a, **4b**, and **4c** show the areal capacitance ***C*** of the ILLis, ILNas, and ILCas, respectively, as a function of frequency. ***C*** is difined by the following equation [18, 20],

$$C = \frac{1}{2\pi f |Z_{\mathrm{im}}|}, \qquad (3)$$

where f and Z_{im} are the frequency of input signal and the imaginary part of the impedance, respectively. The PIL shows the capacitance of 5.4 μF/cm^2, which retains same level up to 10 kHz. Influence of the doping of metal ions is obvious in high frequency regime more than 1

kHz, and the ***C***s of the ILLi, ILNass, and ILCas are smaller than that of the PIL. The reduction of the ***C***s might be attributed to decrease of the ionic conductivity by increase of the viscosity. **Figure 4d**, **4e**, and **4f** summarize the C_s of the ILLis, ILNas, and ILCas at 1 Hz, respectively. The ***C***s slightly decrease with increases in the wight ratio of the salts, and the changes of the ***C***s by doping the metal ions are not significant compared with the ionic conductivity.

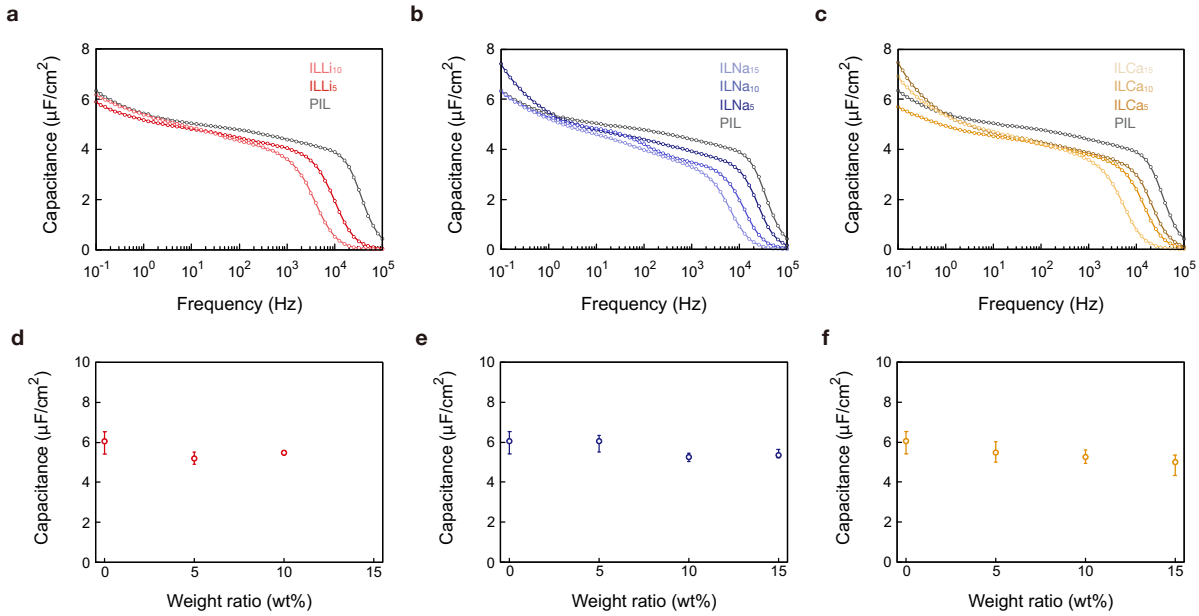

Figure 4. Capacitances curves of the ILs with the (d) Li, (e) Na, and (f) Ca ions with a frequency ranging from 10 mHz to 1 MHz. Changes of capacitances of the ILs with respect to weight ratios of the (d) Li, (e) Na, and (f) Ca salts at 1 Hz.

2.4. Potential window.

We performed linear sweep voltammetry to investigate the influence of the metal ions on the electrochemical stability. We used a three-electrode cell using a glassy carbon electrode, Pt electrode, and Ag/Ag^+ electrode as a working, counter, and reference electrode, respectively. **Figure 5** shows the LSV curves of the ILs at a scan rate of 5 mV/s. A certain cutoff current to determine potential windows leads to unreasonably large potential windows with such low current densities ascribed to the low ionic conductivity of the ILs. The potential windows are

elucidated by the intersection of the lines in faradic and non-faradic regions obtained by a linear fitting method as previously reported [21]. **Table 3** displays the potential windows, cathodic limits, and anodic limits of the ILs. The ILs show the potential windows more than 2.9 V, and such a large potential window is favorable for biodegradable ionic devices. The increases in the weight ratio of the metal ions enable to slightly expand the potential windows by a few hundreds of mV without detection of current peaks within the potential windows.

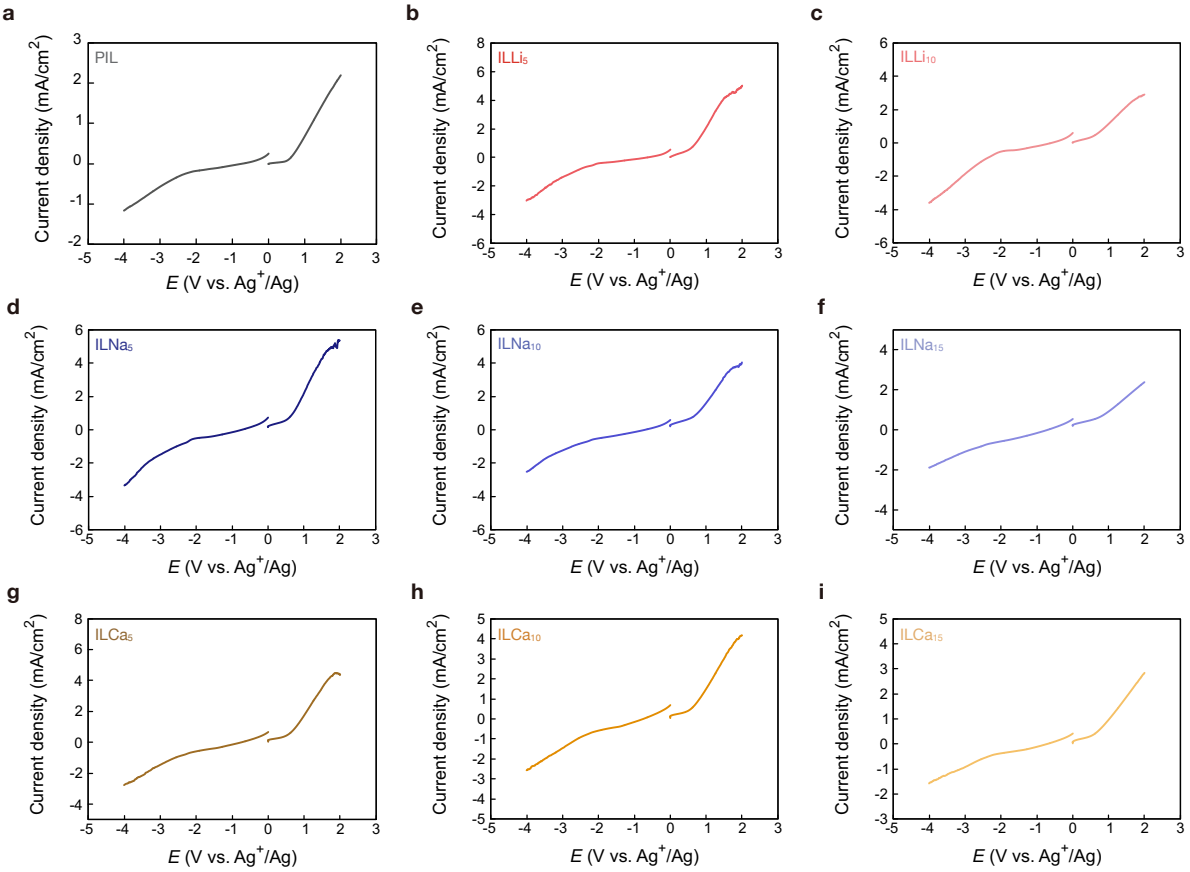

Figure 5. linear sweep voltammetry curves of the (a) PIL, (b) $ILLi_5$, (c) $ILLi_{10}$, (d) $ILNa_5$, (e) $ILNa_{10}$, (f) $ILNa_{15}$, (g) $ILCa_5$, (h) $ILCa_{10}$, and (i) $ILCa_{15}$ at a scan rate of 5 mV/s.

Table 3. potential windows, cathodic and anodic limits of ILs

Ionic liquid	Metal ion	Potential window (V)	Cathodic limit (V vs. Ag/Ag^+)	Anodic limit (V vs. Ag/Ag^+)
PIL	-	3.0	−2.4	0.59
IG	-	3.4	-	-
$ILLi_5$	Li	3.2	−2.5	0.68
$ILLi_{10}$	Li	2.9	−2.3	0.65
$ILLi_{15}$	Li	-	-	-
$ILNa_5$	Na	3.4	−2.8	0.61
$ILNa_{10}$	Na	3.5	−2.8	0.75
$ILNa_{15}$	Na	3.5	−2.7	0.81
$ILCa_5$	Ca	3.2	−2.6	0.63
$ILCa_{10}$	Ca	3.1	−2.5	0.60
$ILCa_{15}$	Ca	3.1	−2.4	0.70

2.5. Characteristics of ionic gel.

We investigated the electrochemical and mechanical characteristics of the IG as displayed in **Fig. S1a** and **S1b**. The precursor of the IG was prepared by mixing the PIL, PVA, and DIW with the weight ratio of PIL:PVA:DIW = 4:1:6 and coated on a glass by the blade-coating method with a blade height of 1 mm. The film of the IG was placed on a fluorine doped tin oxide electrode (FTO, ASONE, NPV-CFT2-7B), followed by drying in a vacuum oven at 1 Pa, 40˚C, for 24 h. We, then, laminated another FTO electrode on top of the IG. **Figure S1c** shows the impedance and phase curves of the IG with respect to frequency by the EIS measurement. The $\boldsymbol{\sigma}$ at 100 kHz is 137 μS/cm^2 according to the equation (2) and 16% smaller than that of the PIL. The $\boldsymbol{C}$ of the IG appears in **Fig. S1d**, replotting its impedance with the equation (3). Its $\boldsymbol{C}$ at 1 Hz is 5.8 μF/cm^2 and remains at the same level as the PIL, $ILLi_5$, and IG while the gelation reduces the conductivity of the IG. As appeared in **Fig. S1e**, the LSV curve of the IG using a two-electrode cell at a scan rate of 5mV/s indicates that the potential window is 3.4 V, and such a large potential window is favorable for electrochemical devices. As for mechanical characteristics, we stretched the IG using a tensile tester as shown in **Fig. S1f**. The fracture

strain and Young's modulus of the IG are 192 % and 666 kPa, respectively, where the values are average in three times tests. Such stretchability and softness are beneficial for stretchable electronics.

2.6. Biodegradability test.

A study on the biodegradability of the ILs, including PIL, ILLis, ILNas, ILCas, and IG was performed according to OECD guidelines for testing of chemicals (OECD 301C modified MITI test (I)) [22]. The samples were added into basal culture media, and the solutions were incubated at 25˚C for 28 days, where a coulometer (Ohkura Electric Co., Ltd., OM3100A) monitored biological oxygen demand BOD in the samples. It should be noted that the tests were performed on three groups; group A includes the PIL and IG; group B includes the $ILLi_5$, $ILLi_{10,}$ $ILNa_5$, and $ILNa_{10}$; group C includes the $ILNa_{15}$, $ILCa_{5,}$ $ILCa_{10}$, and $ILCa_5$. As shown in **Fig. 6a** and **6b**, the BOD of the PIL and IG rapidly increase in 4 days and gradually rise as the day passes. Finally, the BOD of the PIL and IG reaches 152.9 mg/l and 123.7 mg/l, respectively, and the PIL shows a high BOD compared with the IG. The BOD of the ILLis, ILNas, and ILCas depict the same curves as that of PIL as shown in **Fig. S2**. In 28 days, The $ILLi_5$, $ILLi_{10,}$ $ILNa_5$, $ILNa_{10,}$ $ILNa_{15}$, $ILCa_{5,}$ $ILCa_{10}$, and $ILCa1_{15}$ show the BODs of 157.7 mg/l, 151.5 mg/l, 152.4 mg/l, 149.4 mg/l, 166.4 mg/l, 176.1 mg/l, 167.5 mg/l, and 115.0 mg/l, respectively.

biodegradability BD is defined as a ratio of BOD in regard to theoretical oxygen demand ThOD and written as the following equation,

$$BD = \frac{BOD(\text{day}) - B(\text{day})}{ThOD} \times 100\ (\%), \qquad (4)$$

where BOD(day) and B(day) are daily biological oxygen demand and oxygen uptake in the blank inoculum control, respectively. The derivation of ThOD is discussed in supplementary information (see SI). **Figure 6c** and **6d** show the biodegradability of PIL ($BD_{\text{BOD\_PIL}}$) and IG ($BD_{\text{BOD\_IG}}$), respectively. The $BD_{\text{BOD\_PIL}}$ reaches 70% in 6 days whereas the maximum $BD_{\text{BOD\_IG}}$

is 54% within 28 days. PVA is known as a biodegradable polymer [23], but the biodegradation rate of PVA is moderate under an environment of the OECD test [24]. The PVA, therefore, could lead to the slow biodegradation of the IG. The BD curves of the ILLi, ILNa, and ILCa are displayed in **Fig. S3**. The BDs are more than 75% after the test, which indicates that the type of alkaline metal ions and the density do not hinder the degradation process of active sludge. The difference in the activity of the sludge of the test groups could lead to the higher BDs for the $ILNa_{15}$, $ILCa_5$, $ILCa_{10}$, and $ILCa_{15}$ than those of the PIL, $ILLi_5$, $ILLi_{10}$, $ILNa_5$, and $ILNa_{10}$.

The biodegradability of the samples is also evaluated by dissolved organic carbon (DOC) before and after the test. The DOC degradation is defined as

$$\mathrm{DOC} = \frac{W_\mathrm{B} - W_\mathrm{A}}{W_\mathrm{B}} \times 100\ (\%), \qquad (5)$$

where W_A and W_B are the masses of residual carbon of the samples incubated with the basal culture medium and activated sludge, and with water alone, respectively. As summarized in **Table 4**, the DOC biodegradation of PIL is 96.3%, and ILLis, ILNas, and ILCas show high biodegradation levels of over 92%, which agrees with the high degradation in the BOD tests. Based on the BOD and DOC tests, the alkaline metal ions provide no negative influence on the biodegradation of the PIL by the active sludge. The biodegradation of the IG is, meanwhile, 84.1%, which value is 10% lower than those of the ILs. Nonetheless, the PVA is widely known as a biodegradable polymer, and a prolonged closed bottle test revealed 62% biodegradation of PVA (MW = 22 000) at day 108 [24]. The IG is, therefore, a promising material for transient ionics. **Table S1** is the summary of the properties of the IL and IG, the ionic conductivity at 100 kHz, potential windows, cathodic and anodic limits and comparison with the previous works[21, 25]. Although the ionic conductivity and potentials windows of the ILs in this work a few order magnitudes smaller than those in the precious works, the ready biodegradability and bio-derived materials are beneficial for environmental sensing and health monitoring.

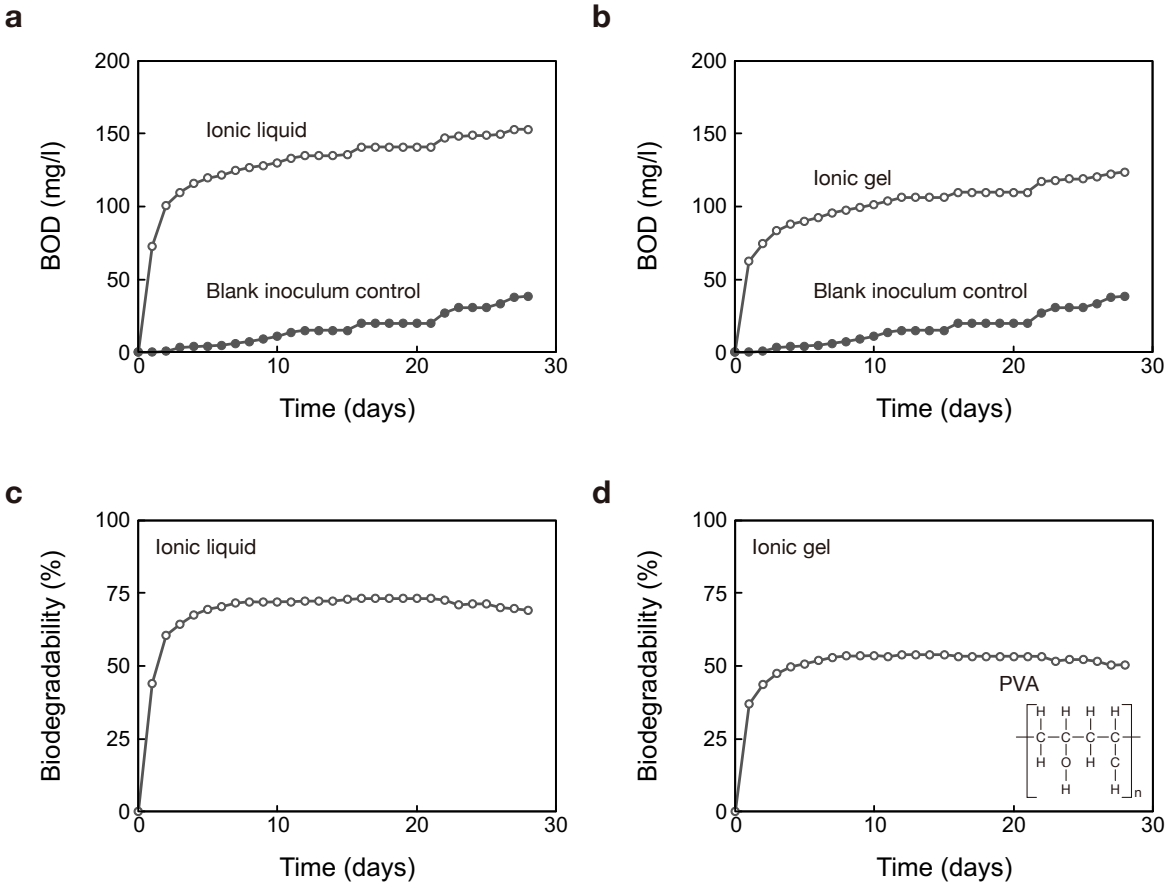

Figure 6. Results of biological oxygen demand (BOD) test. BOD of the (a) ionic liquid and (b) ionic gel. Biodegradability of (c) ionic liquid and (d) ionic gel, calculated by BOD and theoretical oxygen demand ThOD.

Table 4. Summary of the BOD and DOC tests on the ionic liquids and ionic gel.

Sample	*BD*	W_A (mg/l)	W_B (mg/l)	DOC (%)	Classification
PIL	69.1%	1.7	44.6	96.3	Ready Biodegradability
IG	51.4%	5.2	33.0	84.1	Biodegradable
$ILLi_5$	77.5%	2.6	41.8	93.7	Ready Biodegradability
$ILLi_{10}$	74.5%	2.0	39.6	95.0	Ready Biodegradability
$ILLi_{15}$	-	-	-	-	-
$ILNa_5$	73.8%	2.3	37.9	94.0	Ready Biodegradability
$ILNa_{10}$	73.5%	2.0	28.1	92.9	Ready Biodegradability
$ILNa_{15}$	100.2%	2.3	42.1	94.6	Ready Biodegradability
$ILCa_5$	102.3%	2.8	44.3	93.7	Ready Biodegradability

$ILCa_{10}$	98.2%	2.5	43.0	94.3	Ready Biodegradability
$ILCa_{15}$	94.0%	2.8	41.6	93.3	Ready Biodegradability

2.7. Electrochromic device using ionic gel with Li ions

As for the practical application of the ILs, we adapt an IG including the $ILLi_{10}$ ($IGLi_{10}$) as an electrolyte for an electrochromic device (EC). The fabrication of the EC begins with sputtering to deposit a 300-nm-thick WO_3 layer on a glass substrate coated with FTO. The $IGLi_{10}$ was placed on the FTO with WO_3, followed by drying in a vacuum oven at 1 Pa, 40˚C, for 24 h. We laminated a FTO electrode without WO_3 on the $IGLi_{10}$ to produce the EC as shown in **Fig. 7a**. Upon application of a negative voltage of −2.5 V on WO_3, Li ions intercalate into the crystal of WO_3 to form Li_xWO_3 ($0 < x < 1$) written as [26]

$$WO_3 + xLi^+ + xe^- \leftrightarrow Li_xWO_3. \quad (7)$$

The intercalation of Li ions results in a change of the color of WO_3 from pale yellow to dark blue as shown in **Fig. 7b**. Whereas the cyclic voltammetry (CV) curves at 5 mV/s do not show anodic peaks with a voltage range of 2.0 V or less, anodic peaks evolve and are obvious with a voltage range more than 2.5 V as shown in **Fig. 7c**. With the increase of scan rates, cathodic peaks at around 0 V to −1.0 V are obvious, and corresponding anodic peaks become high as shown in **Fig. 7d**. The developed EC needs 2.5 V or more to change its color, and the voltage are relatively high, compared with those in previous works[27]. The ECs with WO_3 in previous works adapted nother electrochemical active layers or species, for example, polyaniline[27a], dimethyl ferrocene[27b], and molybdenum oxide[28], to form complementary redox systems, where WO_3 and the other electrochemical active layers/species are oxidized and reduced upon application of voltage, respectively, and vice versa. The complementary redox systems

accelerate the redox reaction of WO_3 and allow low operational voltage for electrochromic devices. Zhang et al., reports an electrochromic device with an electrolyte (PVA and H_2SO_4) and a pair of the working electrode with the WO_3 layer and ITO counter electrode show a large operational voltage of more than 2.0 V to change its color by intercalation of hydrogen (H) ions into the WO_3 crystal[28]. Meanwhile, the ITO counter electrode with molybdenum oxide accelerates the intercalation of H ions at a WO_3 working electrode, and the electrochromic device shows the change of color at 0.5 V. The electrochromic device in this work has the single electrochemical active layer, WO_3, leading to the high operational voltage to intercalate the Li ions into the WO_3 crystal. **Figure 7e** and **7f** show chronoamperometry curves with alternative voltages of −2.5 V and 2.5 V on the working electrode and corresponding spectra of transmittance of the device under colored and bleached state. The transmittance in the colored state reduces by less than 30% in the visible spectrum. Please note that the noise at 750 nm is ascribed to the mechanical motion of optical components in an UV-Vis spectrophotometer (V700, JASCO). Coloration efficiency η is calculated using the following equation,

$$\eta = \frac{\Delta OD}{\Delta Q} = \frac{\log \frac{T_b}{T_c}}{\Delta Q}. \quad (7)$$

where ΔOD, ΔQ, T_b, and T_c are the variation of optical density, the charge consumed for coloration, and the transmittances in the bleached and colored states, respectively. The ΔOD at 630 nm and the ΔQ are 0.23 and 12 mC/cm^2, respectively. We assume a linear relation between ΔOD and ΔQ, and hence the η is 18 cm^2/C. The η is a few times smaller than those in previous works, which is ascribed to the small ΔOD by the single redox system in this work. Adapting the complementary redox systems could allow us to develop the EC with the high η and low operational voltage.

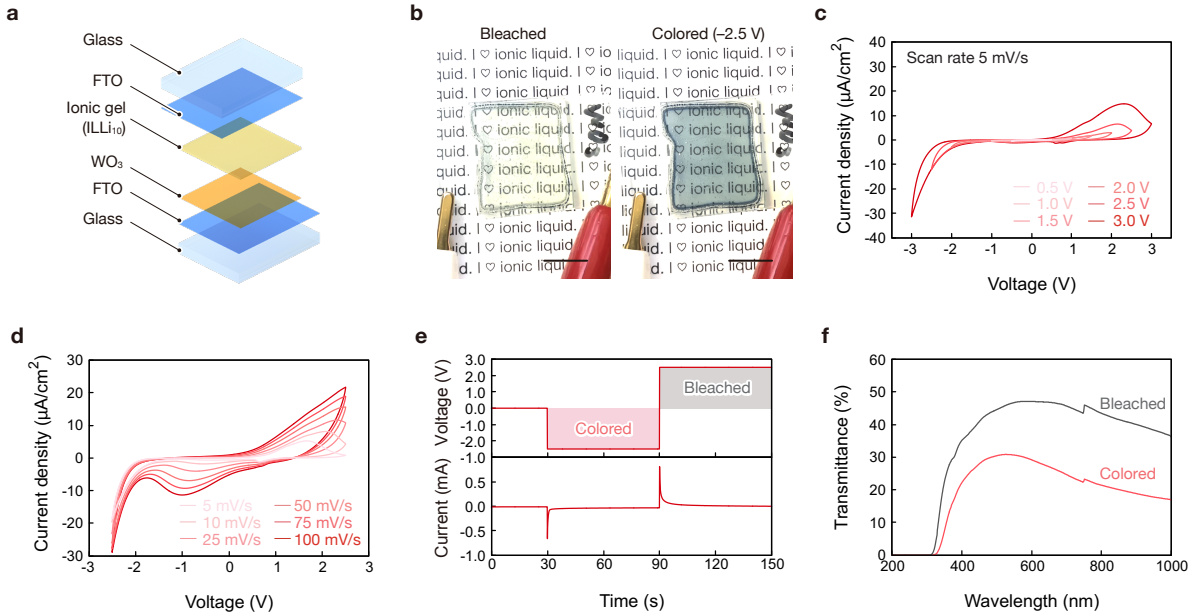

Figure 7. (a) Schematic of EC device using IGLi$_{10}$. (b) The photographs of the EC device in bleached and colored states. (c) CV curves with voltage ranges from ±0.5 V to ±3.0 V at a scan rate of 5 mV/s. (d) CV curves with a voltage range from −2.5 V to 2.5 V at a scan rate from 5 mV/s to 100 mV/s. (e) A chronoamperometry curve to color and bleach the EC device at −2.5 V and 2.5 V, respectively, for 60 s, and (f) the corresponding transmittance of the EC device in the colored and bleached states.

3. Conclusion

We successfully doped metal ions into the PIL by dissolving [Li][Lac], [Na][Lac], or [Ca][Lac], into the PIL. The PIL accommodates 10wt% Li, 15wt% Na and Ca ions, and the ILs with metal ions retain the same level of the capacitance and potential window of the PIL. The ILs solely consist of materials that exist in human bodies, and the biodegradability tests confirm that the PIL, ILLi, ILNa, and ILCa show the ready biodegradability regardless of the metal ions. Although the IG is not classified as the ready biodegradability, its high biodegradability in the DOC tests indicates that the ILs and IG are great candidates to fabricate wearable and transient

devices which decompose in the human body and environment. The $ILLi_{10}$ was used as the electrolyte for the electrochromic device that changes the color by the intercalation of the Li ions into the WO_3 crystal. The future application using the ILs and the IG includes power sources, sensors, and displays, that disappear without toxic substances after use.

Experimental Section

Preparation of the IL with metal ions and IG: The materials, 2-hydroxyethyl-trimethylammonium L-(+)-lactate (product number: 670391, Sigma Aldrich), lithium-L-lactate (product number: 120-03632, FUJIFILM Wako Pure Chemical Company), sodium-L-lactate (product number: 71718-10G, Sigma Aldrich), and calcium lactate (fluorochem, product number: 533047) were used as received. The IL and salts were kept in the vacuum oven for 24 h at 70˚C to repel the residual moisture. We, then, added the salt into the IL, where the weight ratios of the salts are 5wt%, 10wt%, and 15wt% in regard to the IL; the mixtures were stirred vigorously until the salts dissolved. The homogenous solution was kept in the oven at 60˚C for 3 h to remove bubbles, followed by vacuum annealing for 24 h at 70˚C and to repel the residual moisture. As for the IG, its precursor is prepared by mixing the PIL, PVA, and DIW with the ratio PIL:PVA:DIW = 4:1:6. We added the DIW and PVA into a glass bottle and heated in an oven at 110˚C to dissolve the PVA. The PIL is added into the solvent followed by heating at 110˚C for 3 h. The precursor was, then, coated on a glass by the blade-coating method with a blade height of 0.5 mm to obtain the IG.

Electrochemical measurements for EIS: The fabrication of the electrodes began with cutting glass substrates and making holes in the glass substrate to inject the ILs. The glass substrates were, then, cleaned with organic solvents, acetone, ethanol, and deionized water (DIW), followed by cleaning using piranha solution containing 95% sulfuric acid (H_2SO_4) and 30% hydrogen peroxide (H_2O_2) with a volume ratio of H_2SO_4:H_2O_2 = 2:1. Chromium and gold with

thicknesses of 20 nm and 200 nm, respectively, were deposited on the glass substrate by sputtering to make electrodes using a stencil mask patterned with a laser cutter. A polyimide tape was laminated on the electrodes to render the contact area of 1 cm^2 between the ILs and electrodes. A pair of electrodes were assembled using a glass spacer with a thickness of 500 μm, followed by injection of the ILs through the holes. EIS measurements were conducted using an EIS module (FRA32M, Autolab).

Electrochemical measurements for potential window: Residual oxygen in the ILs was purged by bubbling with N_2 gas for 30 minutes before LSV. LSV for the potential window measurement was performed with the three-electrode cell, using the glassy carbon (EC FRONTIER CO., LTD, catalog ID: GC-3155), Ag/Ag^+ (EC FRONTIER CO., LTD, catalog ID: RE-12A), and Pt wire electrode (EC FRONTIER CO., LTD, catalog ID: CE-300) as a working, reference, and counter electrodes, respectively, where the reference electrode was filled with an acetonitrile electrolyte composed of 10 mM $AgNO_3$ and 100 mM NBu_4ClO_4. LSV was carried out with a potentiostat (PGSTAT204, Autolab).

Electrochromic device: The precursor of the $IGLi_{10}$ is prepared by mixing the PIL, PVA, and DIW with the ratio $ILLi_{10}$:PVA:DIW = 4:1:6. We added the DIW and PVA into a glass bottle and heated in an oven at 110°C to dissolve the PVA. The $ILLi_{10}$ is added into the solvent followed by heating at 110°C for 3 h. The precursor was, then, coated on a glass by the blade-coating method with a blade height of 0.5 mm to obtain the $IGLi_{10}$. A 300-nm-thick WO_3 layer was deposited on a glass substrate coated with FTO using sputtering. The $IGLi_{10}$ film was placed on the FTO with WO_3, followed by drying in a vacuum oven at 1 Pa, 50°C, for 24 h to repel the moisture in the $IGLi_{10}$ film. We laminated another FTO electrode on the $IGLi_{10}$ to form the EC. A potentiostat/galvanostat (PGSTAT204, Autolab) was used to characterize the EC.

Biodegradation test: The biodegradability test was performed abide a standard protocol, OECD 301C modified MITI test (I). Before the test, residual moisture in the PIL and IG was removed by vacuum annealing for 24 hours at 50˚C. A 1 L basal culture medium was prepared by mixing water and four 3 mL solutions A, B, C, and D, respectively. The 100 mL solution A included dipotassium hydrogen phosphate of 2.18 g, potassium dihydrogen phosphate of 0.85 g, disodium hydrogen phosphate 12-water of 4.46 g, ammonium chloride of 0.17 g; the 100 mL solution B included magnesium sulfate heptahydrate of 2.25 g; the 100 mL solution C included calcium chloride anhydrous 2.75 g; the 100 mL solution D included ferric chloride iron (III) chloride hexahydrate 0.025g. The BOD tests were performed on the samples with the 300 mL basal culture medium and 9 mg activated sludge and blank inoculum control that consists of the 300 mL basal culture medium and 9 mg activated sludge. The samples were incubated for 28 days at 25±1˚C, where a coulometer (Ohkura Electric Co., Ltd., OM3100A) monitors oxygen consumption and supplies oxygen which is the same amount as that is consumed. After the incubation, the amounts of residual carbon in the samples are analyzed using a TOC measurement (Analytik Jena, multi N/C 3100).

AUTHOR INFORMATION
Corresponding author
*E-mail: santa@tohoku.ac.jp
ORCID
Shunsuke Yamada: 0000-0002-9084-2070
NOTES
The authors declare no competing financial interest.

Acknowledgements
This work was supported in part by JSPS Grant-in-Aid for Early-Career Scientists 22K14213, Japan, and the Toyota Physical and Chemical Research.

Received: ((will be filled in by the editorial staff))
Revised: ((will be filled in by the editorial staff))
Published online: ((will be filled in by the editorial staff))

References

[1] S. W. Hwang, H. Tao, D. H. Kim, H. Y. Cheng, J. K. Song, E. Rill, M. A. Brenckle, B. Panilaitis, S. M. Won, Y. S. Kim, Y. M. Song, K. J. Yu, A. Ameen, R. Li, Y. W. Su, M. M. Yang, D. L. Kaplan, M. R. Zakin, M. J. Slepian, Y. G. Huang, F. G. Omenetto, J. A. Rogers, *Science* **2012**, 337, 1640.

[2] a) S. Yamada, H. Toshiyoshi, *ACS Appl Mater Interfaces* **2020**, 12, 36449; b) S. K. Kang, R. K. J. Murphy, S. W. Hwang, S. M. Lee, D. V. Harburg, N. A. Krueger, J. H. Shin, P. Gamble, H. Y. Cheng, S. Yu, Z. J. Liu, J. G. McCall, M. Stephen, H. Z. Ying, J. Kim, G. Park, R. C. Webb, C. H. Lee, S. J. Chung, D. S. Wie, A. D. Gujar, B. Vemulapalli, A. H. Kim, K. M. Lee, J. J. Cheng, Y. G. Huang, S. H. Lee, P. V. Braun, W. Z. Ray, J. A. Rogers, *Nature* **2016**, 530, 71.

[3] L. Yin, X. Huang, H. Xu, Y. Zhang, J. Lam, J. Cheng, J. A. Rogers, *Adv Mater* **2014**, 26, 3879.

[4] a) C. Abrusci, J. Palomar, J. L. Pablos, F. Rodriguez, F. Catalina, *Green Chemistry* **2011**, 13, 709; b) S. Yamada, H. Toshiyoshi, *Small* **2018**, 14, e1800937.

[5] S. Yamada, T. Sato, H. Toshiyoshi, *Applied Physics Letters* **2017**, 110.

[6] S. Yamada, *ACS Appl Mater Interfaces* **2022**, DOI: 10.1021/acsami.2c00915.

[7] a) D. Chao, H. J. Fan, *Chem* **2019**, 5, 1359; b) H. Huang, M. Niederberger, *Nanoscale* **2019**, 11, 19225.

[8] a) H. W. Sheng, J. J. Zhou, B. Li, Y. H. He, X. T. Zhang, J. Liang, J. Y. Zhou, Q. Su, E. Q. Xie, W. Lan, K. R. Wang, C. J. Yu, *Sci Adv* **2021**, 7; b) T. Brezesinski, J. Wang, S. H. Tolbert, B. Dunn, *Nat Mater* **2010**, 9, 146.

[9] B. T. Liu, X. M. Shi, X. Y. Lang, L. Gu, Z. Wen, M. Zhao, Q. Jiang, *Nat Commun* **2018**, 9, 1375.

[10] a) G. Lee, S.-K. Kang, S. M. Won, P. Gutruf, Y. R. Jeong, J. Koo, S.-S. Lee, J. A. Rogers, J. S. Ha, *Advanced Energy Materials* **2017**, 7; b) H. Lee, G. Lee, J. Yun, K. Keum, S. Y. Hong, C. Song, J. W. Kim, J. H. Lee, S. Y. Oh, D. S. Kim, M. S. Kim, J. S. Ha, *Chemical Engineering Journal* **2019**, 366, 62; c) L. Yin, H. Y. Cheng, S. M. Mao, R. Haasch, Y. H. Liu, X. Xie, S. W. Hwang, H. Jain, S. K. Kang, Y. W. Su, R. Li, Y. G. Huang, J. A. Rogers, *Advanced Functional Materials* **2014**, 24, 645.

[11] a) E. Karpierz, L. Niedzicki, T. Trzeciak, M. Zawadzki, M. Dranka, J. Zachara, G. Z. Zukowska, A. Bitner-Michalska, W. Wieczorek, *Sci Rep* **2016**, 6, 35587; b) S. Matsuura, M. Shibata, J. Han, K. Fujii, *ACS Applied Polymer Materials* **2020**, 2, 1276; c) S. Ono, K. Miwa, S. Seki, J. Takeya, *Organic Electronics* **2009**, 10, 1579; d) S. Ono, K. Miwa, S. Seki, J. Takeya, *Applied Physics Letters* **2009**, 94.

[12] W. H. W. Tang, D. Y. Li, S. L. Hazen, *Nat Rev Cardiol* **2019**, 16, 137.

[13] a) B. Faubert, K. Y. Li, L. Cai, C. T. Hensley, J. Kim, L. G. Zacharias, C. Yang, Q. N. Do, S. Doucette, D. Burguete, H. Li, G. Huet, Q. Yuan, T. Wigal, Y. Butt, M. Ni, J. Torrealba, D. Oliver, R. E. Lenkinski, C. R. Malloy, J. W. Wachsmann, J. D. Young, K. Kernstine, R. J. DeBerardinis, *Cell* **2017**, 171, 358; b) S. Hui, J. M. Ghergurovich, R. J. Morscher, C. Jang, X. Teng, W. Lu, L. A. Esparza, T. Reya, Z. Le, J. Yanxiang Guo, E. White, J. D. Rabinowitz, *Nature* **2017**, 551, 115.

[14] https://ods.od.nih.gov/factsheets/Choline.

[15] J. D. Rabinowitz, S. Enerback, *Nat Metab* **2020**, 2, 566.

[16] S. Yamada, *Small* **2023**, DOI: 10.1002/smll.202205598e2205598.

[17] Z. Cao, H. Liu, L. Jiang, *Materials Horizons* **2020**, 7, 912.

[18] A. F. Visentin, M. J. Panzer, *ACS Appl Mater Interfaces* **2012**, 4, 2836.

[19] J. Serra Moreno, G. Maresca, S. Panero, B. Scrosati, G. B. Appetecchi, *Electrochemistry Communications* **2014**, 43, 1.

[20] M. Matsumoto, S. Shimizu, R. Sotoike, M. Watanabe, Y. Iwasa, Y. Itoh, T. Aida, *J Am Chem Soc* **2017**, 139, 16072.
[21] M. P. Mousavi, B. E. Wilson, S. Kashefolgheta, E. L. Anderson, S. He, P. Buhlmann, A. Stein, *ACS Appl Mater Interfaces* **2016**, 8, 3396.
[22] https://doi.org/10.1787/9789264070349.
[23] a) L. Chen, T. Qiang, X. Chen, W. Ren, H. J. Zhang, *ACS Applied Polymer Materials* **2021**, 4, 357; b) E. Chiellini, A. Corti, S. D'Antone, R. Solaro, *Progress in Polymer Science* **2003**, 28, 963; c) S. Feng, S. Cao, Z. Tian, H. Zhu, D. Kong, *ACS Appl Mater Interfaces* **2019**, 11, 45844; d) E. S. Hosseini, S. Dervin, P. Ganguly, R. Dahiya, *ACS Appl Bio Mater* **2021**, 4, 163; e) W. Niu, Y. Zhu, R. Wang, Z. Lu, X. Liu, J. Sun, *ACS Appl Mater Interfaces* **2020**, 12, 30805.
[24] C. G. Vanginkel, C. A. Stroo, *Ecotox Environ Safe* **1992**, 24, 319.
[25] G. B. Appetecchi, M. Montanino, D. Zane, M. Carewska, F. Alessandrini, S. Passerini, *Electrochimica Acta* **2009**, 54, 1325.
[26] M. Wang, Y. Chen, B. Gao, H. Lei, *Advanced Electronic Materials* **2019**, 5.
[27] a) W. Q. Wang, X. L. Wang, X. H. Xia, Z. J. Yao, Y. Zhong, J. P. Tu, *Nanoscale* **2018**, 10, 8162; b) T. Y. Yun, X. Li, J. Bae, S. H. Kim, H. C. Moon, *Materials & Design* **2019**, 162, 45.
[28] W. Zhang, H. Li, C. J. Firby, M. Al-Hussein, A. Y. Elezzabi, *ACS Appl Mater Interfaces* **2019**, 11, 20378.